nature climate change

LETTERS

https://doi.org/10.1038/s41558-017-0008-6

Increasing frequency of extremely severe cyclonic storms over the Arabian Sea

Hiroyuki Murakami[1,2*], Gabriel A. Vecchi[3,4] and Seth Underwood[1]

In 2014 and 2015, post-monsoon extremely severe cyclonic storms (ESCS)—defined by the WMO as tropical storms with lifetime maximum winds greater than 46 m s^{-1}—were first observed over the Arabian Sea (ARB), causing widespread damage. However, it is unknown to what extent this abrupt increase in post-monsoon ESCSs can be linked to anthropogenic warming, natural variability, or stochastic behaviour. Here, using a suite of high-resolution global coupled model experiments that accurately simulate the climatological distribution of ESCSs, we show that anthropogenic forcing has likely increased the probability of late-season ECSCs occurring in the ARB since the preindustrial era. However, the specific timing of observed late-season ESCSs in 2014 and 2015 was likely due to stochastic processes. It is further shown that natural variability played a minimal role in the observed increase of ESCSs. Thus, continued anthropogenic forcing will further amplify the risk of cyclones in the ARB, with corresponding socio-economic implications.

In 2014, Cyclone Nilofar, the first extremely severe cyclonic storm (ESCS (tropical storms with lifetime maximum winds greater than 46 m s^{-1} (WMO[1])), was recorded in the Arabian Sea (ARB) (west of 77.5° E in the North Indian Ocean) during the post-monsoon season (October–December) (Fig. 1a). In the following year, two more ESCSs (Cyclones Chapala and Megh) were observed during the post-monsoon season in the ARB (Fig. 1a), causing widespread damage[2]. This was the first instance that more than one ESCS was observed within one year in the ARB (Fig. 1b). These recent severe tropical storms in the ARB have attracted considerable attention from the scientific community, as well as broader society, in terms of the extent to which they were made more likely by anthropogenic forcing, as opposed to intrinsic natural variability. A recent study[3] reported that the increase in anthropogenic black carbon and sulfate emissions might have led to the increase in mean storm intensity in the ARB through a weakening of vertical wind shear (V_s, wind speed difference between the upper and lower troposphere), especially during the pre-monsoon season of April–June. The suggested physical mechanism behind this change is that the observed increase in anthropogenic aerosols in the lower troposphere leads to a reduction in surface insolation in the North Indian Ocean, which in turn leads to a decrease in the meridional gradient of sea surface temperature (SST). This decreased meridional gradient further leads to a weakening of the South Asian Monsoon circulation through the thermal wind relationship, which causes a weakening of V_s. On the other hand, another study[4] argued that the recent increase in pre-monsoon tropical storm intensity in the ARB is mainly being caused by an earlier onset of the South Asian Monsoon, affected by a reversal in the phase of the Pacific Decadal Oscillation (PDO) around 1997. Overall, consensus has not been reached regarding the main cause of the recent increase in pre-monsoon storm intensity in the ARB. Alongside this debate, the recent unprecedented

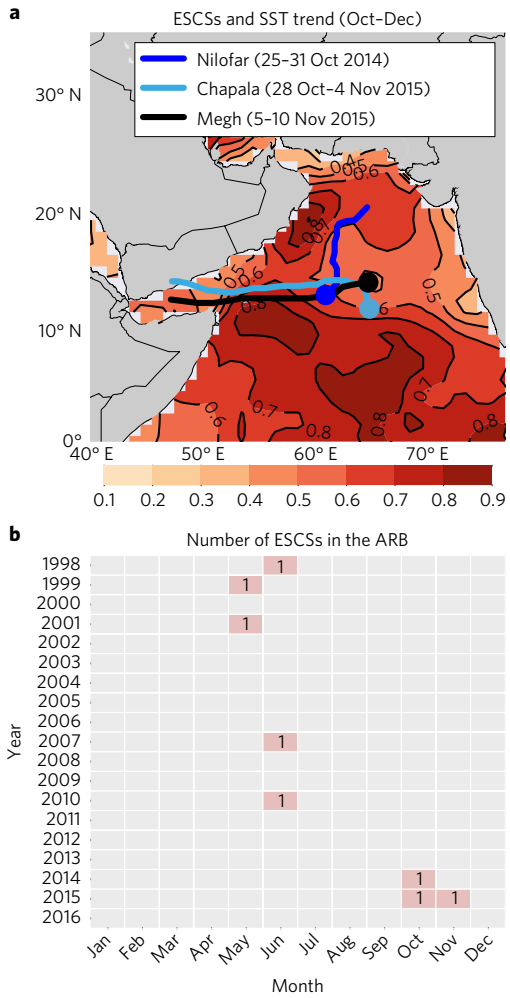

Fig. 1 | Observed ESCSs. a, Observed ESCSs (Nilofar (blue), Chapala (light blue) and Megh (black)) during the post-monsoon season in 2014 and 2015, along with the observed linear trend in SST (Kelvin per 50 years, shading). **b**, Observed number of ESCSs over the ARB for each month for the period 1998–2016.

[1]National Oceanic and Atmospheric Administration/Geophysical Fluid Dynamics Laboratory, Princeton, NJ, USA. [2]Atmospheric and Oceanic Sciences Program, Princeton University, Princeton, NJ, USA. [3]Department of Geosciences, Princeton University, Princeton, NJ, USA. [4]Princeton Environmental Institute, Princeton University, Princeton, NJ, USA. *e-mail: hir.murakami@gmail.com

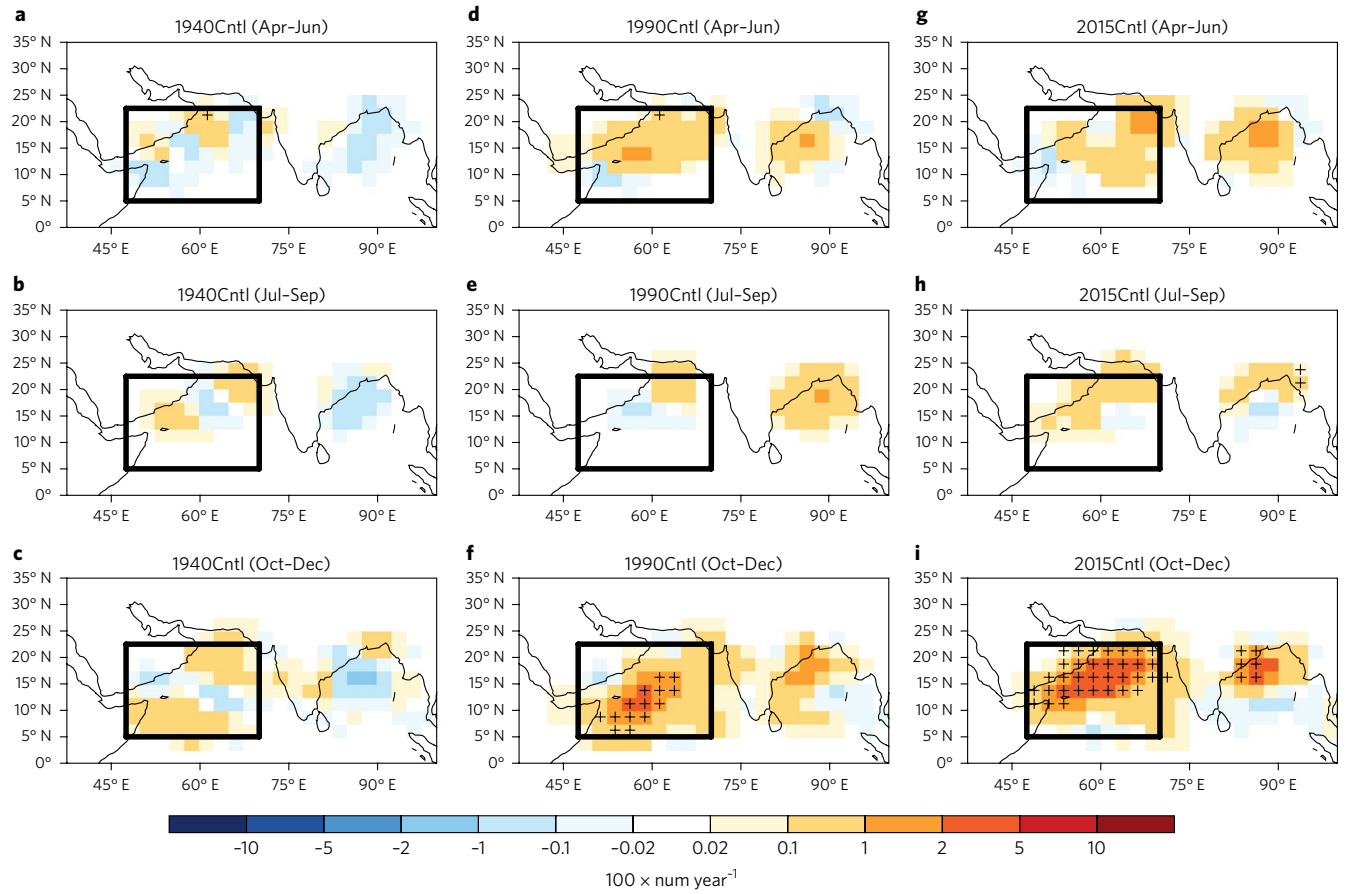

Fig. 2 | Projected changes in the seasonal mean density of ESCSs. a–c, Projected changes in the seasonal mean density of ESCSs by the 1940Cntl relative to the 1860Cntl during the pre-monsoon season (Apr–Jun) (**a**), peak monsoon season (Jul–Sep) (**b**) and post-monsoon season (Oct–Dec) (**c**). **d–f**, As in **a–c**, but for the 1990Cntl. **g–i**, As in **a–c**, but for the 2015Cntl. Crosses indicate that the projected change relative to the 1860Cntl is statistically significant at the 99% confidence level or above (bootstrap method proposed by Murakami et al.[24]). The black box highlights the domain of significant change in the post-season over the ARB.

occurrence of ARB ESCSs in 2014 and 2015 calls for an additional focus on the post-monsoon season. The observed tropical storm activity in the ARB shows a bimodal annual frequency distribution, which peaks during the pre-monsoon and post-monsoon seasons[5]. However, the observed seasonal large-scale conditions are fundamentally different between the two seasons in terms of the direction of low-level wind and V_s (Supplementary Fig. 1). Therefore, the effect of anthropogenic forcing on storm activity could also be different between the two seasons.

Also, long-term analysis of the observed storm record is uncertain given the very limited period of reliable satellite-based data covering the ARB. No satellite covered the entire ARB before 1998, and so storm intensity might have been underestimated because of the oblique view offered by adjacent satellites[6]. However, Fig. 1b reveals that, even after 1998, ESCSs were not observed in the post-monsoon season until 2014, drawing interest as to whether the increase is physically related to anthropogenic warming; indeed, several studies have consistently reported that anthropogenic global warming has increased the mean storm intensity[7].

As a complement to the limited observational record, we use a suite of numerical climate model experiments to address the plausibility and causes of the recent increase in post-monsoon ESCSs in the ARB[8]. The ARB poses a challenge for numerical climate modelling, not only because of its relatively small domain size, but also because of the complex climatic conditions and influences in the region and the general rarity of tropical storm genesis in the ARB. On average, about 1.7 (0.6 during the pre-monsoon season and 0.9 during the post-monsoon season) tropical storms (lifetime maximum surface wind speed $\geq$17.5 m s^{-1}) formed in a year in the ARB during 1979–2015, which is only about 2% of the storm frequency globally. Thus, models with high resolution, fidelity in their climate simulations and the ability to produce multicentennial integrations for the provision of a satisfactory signal-to-noise ratio are required. However, the limited reliability of observations makes it difficult to evaluate model simulations in terms of the interannual variation of storm frequency at the multidecadal timescale. Although many state-of-the-art models succeed in simulating the observed year-by-year variation of tropical storm frequency in the North Atlantic[8–10], they commonly fail to reproduce the equivalent in the North Indian Ocean[10–12]. This failure may result from the imperfect representation of variability in models, the inhomogeneous observed storm record, difficulties with tropical cyclone (TC) detection methods in distinguishing TCs from low-pressure systems (for example, monsoon depressions)[13] or the limited predictability of TC frequency over the region. Another problem with model simulations is that the horizontal resolution of the climate models is still insufficient to reproduce observations of intense storms. Several climate models have been used to conduct future climate projections, and the results commonly suggest that the frequency of weak (intense) storms will decrease (increase) globally in the future[7]. However, most models underestimate the observed TC intensity, especially for major hurricanes (maximum surface wind speed $\geq$50 m s^{-1}) (ref. [7]).

Moreover, little is known about the change in TC activity over the ARB. Murakami et al.[12] conducted multiphysics and multi-SST ensemble climate projections under the IPCC A1B scenario[14] using a 60-km-mesh atmospheric model. The results showed that the mean locations of tropical storms may shift westwards over the North Indian Ocean during the post-monsoon season, which leads to an increased (decreased) frequency of tropical storms over the ARB (Bay of Bengal). However, little is known about possible change in intense storms like ESCSs. The present study aims to bridge that gap.

At the Geophysical Fluid Dynamics Laboratory, we recently developed a new high-resolution global coupled model, called HiFLOR, that broadly reproduces the observed year-by-year variations of the frequency of Category 4 and 5 (C45) hurricanes (maximum wind speed $\geq 58\,m\,s^{-1}$) in the North Indian Ocean ($r \approx 0.4$) as well as in other ocean basins[8,15]. Moreover, HiFLOR simulates the climatological spatial distribution of ESCSs over the ARB reasonably well, as compared with observations, based on a present-day control simulation (Supplementary Fig. 2). Therefore, it is feasible to investigate the factor(s) responsible for the recent increase in ESCSs using HiFLOR. In this study, through a suite of climate simulations, we specifically investigate whether the recent observed increase in ESCSs results from anthropogenic global warming or natural variability.

To estimate the impact of anthropogenic forcing on the frequency of ESCSs over the ARB, we conducted a series of control simulations that prescribed past levels of anthropogenic and natural forcing (Methods). Specifically, we conducted 1860Cntl, 1940Cntl, 1990Cntl and 2015Cntl experiments in which anthropogenic forcing was fixed at years 1860, 1940, 1990 and 2015, respectively (Methods). Figure 2 shows the projected change in the mean ESCS density for each experiment and for each season relative to the 1860Cntl. Although the model response in the 1940Cntl is smaller and not statistically significant for all seasons, the 1990Cntl and 2015Cntl results show significant increases in the occurrence of ESCSs over the ARB during the post-monsoon season only. These projected increases coincide with the recent observed increase in ESCSs over the ARB during the post-monsoon season.

Following Murakami et al.[16,17], we estimated the potential influence of anthropogenic forcing on the frequency of occurrence of ESCSs by computing the empirical probability of exceedance (Methods). In this study, we focus on $P(1)$, representing the probability of the occurrence of a year with one or more ESCSs during the post-monsoon season over the ARB. The grey bars along with the box plots in Fig. 3a clearly indicate a projected significant increase in $P(1)$ for the 1990Cntl and 2015Cntl relative to the 1860Cntl and 1940Cntl. The fraction of attributable risk (FAR) (Methods) for the 2015Cntl and 1990Cntl is 64% and 57%, respectively, which suggests that the increase in the probability of occurrence is attributable to the increase in anthropogenic forcing. We repeated the same analysis for weak storms ($<46\ m\ s^{-1}$), and the results showed no significant changes among the control simulations during the post-monsoon season (Supplementary Fig. 3).

We further computed the conditional $P(1)$—namely, $P(1|Y_{\pm})$ under any phase of a natural mode of variability (that is, Y_+ or Y_-)—to estimate impact of natural variability on the changes in $P(1)$ (Methods). The coloured bars in Fig. 3b reveal the extent to which the different phases of natural variability exert variation in the probability of exceedance. Overall, we obtained diverse and inconsistent results among the control experiments. For example, 2015Cntl (1940Cntl) shows the highest probability during the positive (negative) phase of the PDO. The reason for these diverse results—possibly related to whether the 200–300-year records are short enough to alias the noise and the impact of these internal climate modes on ESCS activity being weak, or to whether the impact of the PDO is sensitive to the base state—remains unclear. The relatively shorter

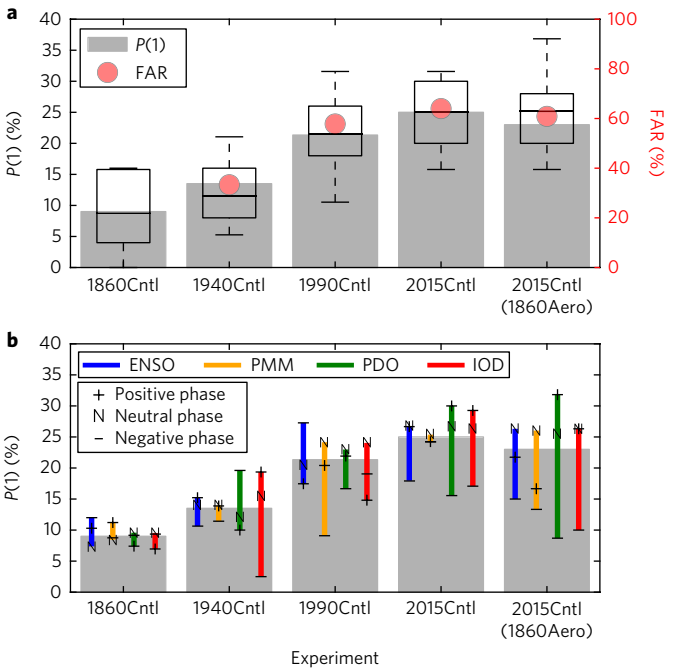

Fig. 3 | Projected probability of exceedance of ESCSs over the ARB during October–December for each experiment. a, $P(1)$, the probability of occurrence of a year with the ESCS number greater than or equal to one during October–December, was obtained with each control experiment using all simulation years (grey bars). The box plots represent the uncertainty in $P(1)$. The boxes represent the range of the 10% and 90% quantiles of $P(1)$ computed from 50-year periods, the horizontal lines show the median value and the dashed bars show the 10% and 90% quantiles computed from 19-year periods. Red dots represent the FAR relative to 1860Cntl. **b**, Grey bars are the same as in **a**. Coloured bars show the range of conditional $P(1)$ induced by natural variability. +, – and N indicate $P(1)$ under the condition of a positive phase, negative phase and neutral phase of natural variability, respectively. Evaluated natural variabilities are ENSO (blue), PMM (orange), PDO (green) and IOD (red). A positive (negative) phase is defined as when a climate index is greater than or equal to $+0.75\sigma$ (less than or equal to -0.75σ).

coloured bars for the longest 600-year 1860Cntl (Fig. 3b) lend weight to the hypothesis that the impact of these potentially predictable modes of climate variability on ESCS activity is weak, which suggests that natural variations in post-monsoon ESCS activity may be largely unpredictable. However, overall, we could not find any clear and robust dependence of the probability of occurrence on these modes of natural variability.

To address the physical mechanism behind the projected increase in ESCSs in the post-monsoon season, we preliminarily investigated several large-scale parameters associated with storm activity. Among them, the projected changes in SST and V_s appear to be responsible for the increase in ESCSs. Figure 4 highlights a marked sea surface warming over the ARB (Fig. 4a), with larger warming relative to the mean change in the tropics (RSST (Supplementary Fig. 4a)), as well as a significant weakening of V_s over the ARB (Fig. 4b). Several previous studies have reported projected increases in TC density and maximum potential intensity such that the SST increases more than in other open oceans[10,18–21]. Similar spatial patterns of the projected changes in the large-scale parameters could also be obtained through future projections with CMIP3 models[19] and CMIP5 models[22]. Figure 4c,d shows the ensemble mean of the projected changes in SST (Fig. 4c) and V_s (Fig. 4d) in 22 CMIP5 models under the RCP8.5 (2006–2025) scenario relative to the

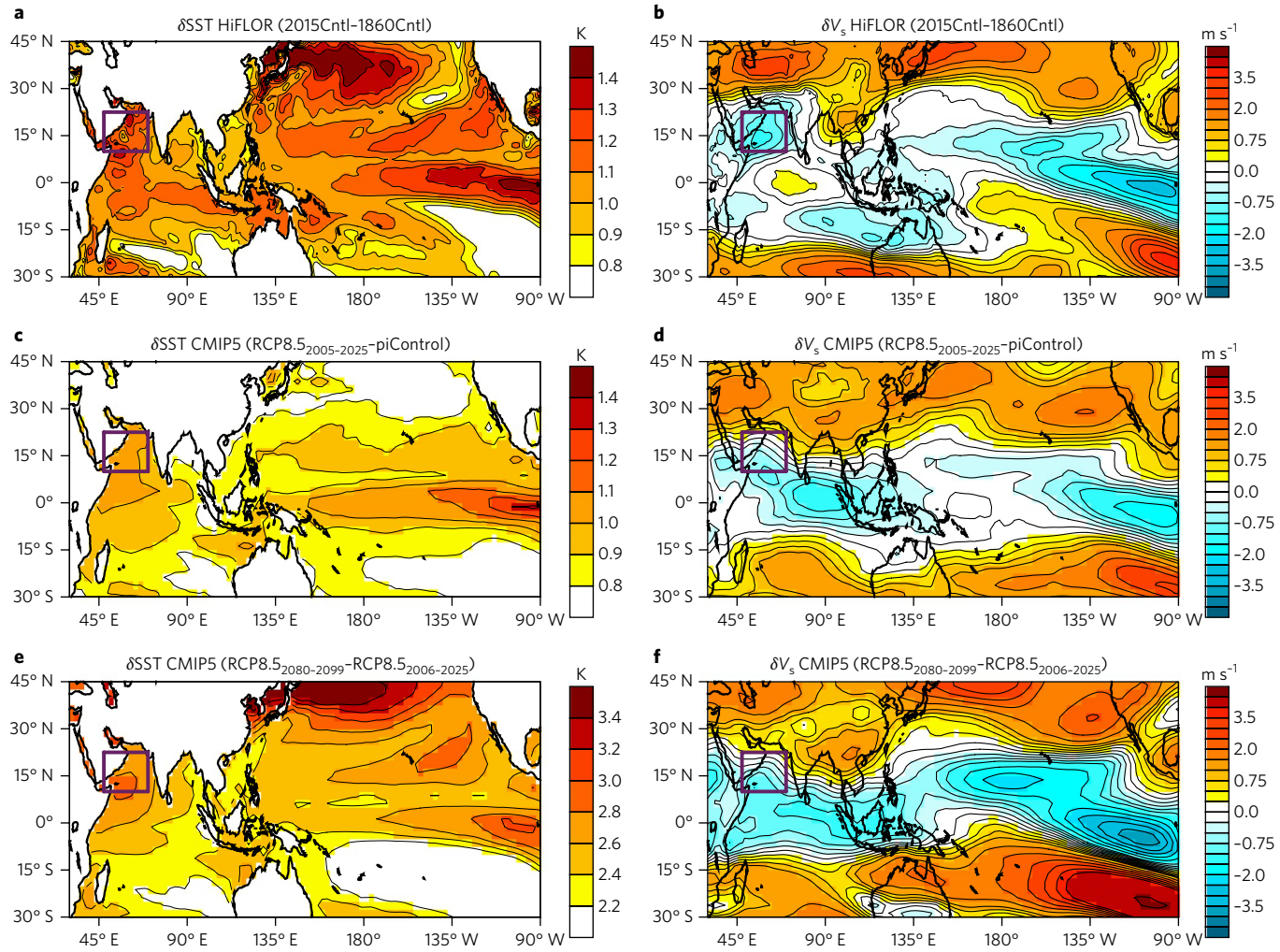

Fig. 4 | Projected changes in seasonal mean SST and V_s. **a**, Projected change in seasonal mean SST (K) by the 2015Cntl relative to the 1860Cntl for October–December. **b**, As in **a**, but for V_s [m s^{-1}]. **c**,**d**, As in **a** and **b**, but for the ensemble mean of 22 CMIP5 models under the RCP8.5 scenario (2006–2025) relative to those of the pre-industrial control experiments (500 years). **e**,**f**, As in **c** and **d**, but for the mean difference between 2080–2099 and 2006–2025 projected by 36 CMIP5 models under the RCP8.5 scenario. The purple rectangles are the domain over the ARB where the ESCSs increased.

pre-industrial control experiments (500 years). The CMIP5 models show a larger warming over the ARB (Supplementary Fig. 4b) that is consistent with the projections by HiFLOR. A larger ARB warming relative to other open oceans has also been reported in century-scale observations[18], in which the largest projected and observed trends in relative SST and potential intensity were found over the tropical part of this region. Moreover, the CMIP5 models also show relatively weaker V_s for the region's increase in ESCSs during the post-monsoon season (Fig. 4d). Similar changes are also projected in the future by the CMIP5 models (Fig. 4e,f), which implies a continuing increase in ARB ECSCs during the post-monsoon season because of weaker shear and warmer SSTs in the future. Similar changes in SST and RSST are also projected during the pre-monsoon season (Supplementary Figs. 4d–f, 5 and 6a,b). However, we could not find any significant decreases in V_s during the pre-monsoon season over the ARB domain where ESCSs increased (Supplementary Figs. 5 and 6c). Consequently, the pre-monsoon season shows a smaller projected increase in $P(1)$ relative to the post-monsoon season (Supplementary Fig. 7).

It is possible that the projected changes in V_s are related to the changes in either the strength or the timing of the onset/retreat of the Indian monsoon. By analysing the changes in the Indian monsoon circulation (Methods), we found that the projected weakening of the winter monsoon circulation is key for the weakening of V_s during the post-monsoon season. Previous literature also reported that state-of-the-art climate models commonly project a weakening of the Indian monsoon circulation in experiments run with anthropogenic forcing[23]. However, we could not find any significant difference in the timing of monsoon onset or withdrawal (Supplementary Fig. 11), although IPCC[23] reported that model agreement is high on an earlier onset and later retreat (that is, longer duration) in future projections. Uncertainty remains in this regard.

As reviewed above, Evan et al.[3] reported that the recent increase in anthropogenic aerosols caused an increase in TC intensity over the ARB through a weakening of V_s. Accordingly, we investigated the influence of aerosols on the frequency of ESCSs. We conducted an additional idealized experiment in which the simulation settings were identical to those in the 2015Cntl, except the anthropogenic aerosols (that is, black carbon, organic carbon, sulfate, etc.) were prescribed at the 1860 level. The increase in aerosols causes a small increase in ESCSs (labelled as '2015Cntl(1860Aero)' in Fig. 3), which is consistent with a previous study[3]. However, the projected impact of aerosols on ESCSs may be underestimated in the model because the model underestimates direct radiative forcing by aerosols over the ARB compared with observations, especially at the surface (Supplementary Fig. 12). Moreover, the model does not

include the indirect effects of aerosols, and so the aerosol forcing is of a smaller amplitude than in the observations. Further refinement of the model's physics is necessary in the future to estimate the effect of aerosols on ECSCs with more precision.

Overall, the suite of high-resolution model experiments carried out in this study indicate that anthropogenic global warming has increased the probability of post-monsoon ESCSs over the ARB, and is one of the major contributors to the recent (2014 and 2015) observations in this regard. The specific occurrence in these two years, but not in other years in recent decades, reflects the interplay between climate change, climate variability and weather. However, the climate simulations do not show any consistent dependency on the phases of natural variability that we explored. Therefore, we believe that stochastic factors (that is, 'weather noise') or unexplored modes of climate variability were key to the precise timing of these events.

Methods

Methods, including statements of data availability and any associated accession codes and references, are available at https://doi.org/10.1038/s41558-017-0008-6.

Received: 19 May 2017; Accepted: 6 October 2017;
Published online: 13 November 2017

References

1. *Tropical Cyclone Operational Plan for the Bay of Bengal and Arabian Sea* WMO/TD-84 (WMO, 2015); www.wmo.int/pages/prog/www/tcp/documents/TCP-21Edition2015_final.pdf
2. Kruk, M. C. Tropical cyclones, North Indian Ocean. *Bull. Amer. Meteorol. Soc.* **97(8)** (Suppl.), 114–115 (2016).
3. Evan, A. T., Kossin, J. P., Chung, C. E. & Ramanathan, V. Arabian Sea tropical cyclones intensified by emissions of black carbon and other aerosols. *Nature* **479**, 94–97 (2011).
4. Wang, B., Xu, S. & Wu, L. Intensified Arabian Sea tropical storms. *Nature* **489**, E1–E2 (2012).
5. Evan, A. T. & Camargo, S. J. A climatology of Arabian Sea cyclonic storms. *J. Clim.* **24**, 140–158 (2011).
6. Kossin, J. P., Olander, T. L. & Knapp, K. R. Trend analysis with a new global record of tropical cyclone intensity. *J. Clim.* **26**, 9960–9976 (2013).
7. Knutson, T. et al. Tropical cyclones and climate change. *Nat. Geosci.* **3**, 157–163 (2010).
8. Murakami, H. et al. Simulation and prediction of Category 4 and 5 hurricanes in the high-resolution GFDL HiFLOR coupled climate model. *J. Clim.* **28**, 9058–9079 (2015).
9. LaRow, T. E., Lim, Y.-K., Shin, D. W., Chassignet, E. P. & Cocke, S. Atlantic basin seasonal hurricane simulations. *J. Clim.* **21**, 3191–3206 (2008).
10. Zhao, M., Held, I. M., Lin, S.-J. & Vecchi, G. A. Simulations of global hurricane climatology, interannual variability, and response to global warming using a 50km resolution GCM. *J. Clim.* **22**, 333–363 (2009).
11. Manganello, J. V. et al. Tropical cyclone climatology in a 10-km global atmospheric GCM: toward weather-resolving climate modeling. *J. Clim.* **24**, 3867–3893 (2012).
12. Murakami, H., Sugi, M. & Kitoh, A. Future changes in tropical cyclone activity in the North Indian Ocean projected by high-resolution MRI-AGCMs. *Clim. Dyn.* **40**, 1949–1968 (2013).
13. Murakami, H. et al. Future changes in tropical cyclone activity projected by the new high-resolution MRI-AGCM. *J. Clim.* **25**, 3237–3260 (2012).
14. IPCC *Climate Change 2007: The Physical Science Basis* (eds Solomon, S. et al.) (Cambridge Univ. Press, Cambridge, 2007).
15. Murakami, H. et al. Seasonal forecasts of major hurricanes and landfalling tropical cyclones using a high-resolution GFDL coupled climate model. *J. Clim.* **29**, 7977–7989 (2016).
16. Murakami, H. et al. Investigating the influence of anthropogenic forcing and natural variability on the 2014 Hawaiian hurricane season. *Bull. Amer. Meteorol. Soc.* **97(12)** (Suppl.), 115–119 (2016).
17. Murakami, H. et al. Dominant role of subtropical Pacific warming in extreme eastern Pacific hurricane seasons: 2015 and the future. *J. Clim.* **30**, 243–264 (2017).
18. Vecchi, G. A. & Soden, B. J. Effect of remote sea surface temperature change on tropical cyclone potential intensity. *Nature* **450**, 1066–1071 (2007).
19. Vecchi, G. A. & Soden, B. J. Increased tropical Atlantic wind shear in model projections of global warming. *Geophys. Res. Lett.* **34**, L08702 (2007).
20. Sugi, M., Murakami, H. & Yoshimura, J. A reduction in global tropical cyclone frequency due to global warming. *SOLA* **5**, 164–167 (2009).
21. Murakami, H., Mizuta, R. & Shindo, E. Future changes in tropical cyclone activity projected by multi-physics and multi-SST ensemble experiments using the 60-km-mesh MRI-AGCM. *Clim. Dyn.* **39**, 2569–2584 (2012).
22. Taylor, K. E., Stouffer, R. J. & Meehl, G. A. An overview of CMIP5 and the experiment design. *Bull. Amer. Meteorol. Soc.* **93**, 485–498 (2012).
23. IPCC *Climate Change 2013. The Physical Science Basis* (eds Stocker, T. F. et al.) (Cambridge Univ. Press, Cambridge, 2013).
24. Murakami, H., Wang, B., Li, T. & Kitoh, A. Projected increase in tropical cyclones near Hawaii. *Nat. Clim. Change* **3**, 749–754 (2013).

Acknowledgements

The authors thank T. L. Delworth and L. Krishnamurthy for their suggestions and comments. H.M. appreciates P.-C. Hsu for her editorial service support. This report was prepared by H.M. under award NA14OAR4830101 from the National Oceanic and Atmospheric Administration (NOAA), US Department of Commerce. The statements, findings, conclusions and recommendations are those of the authors and do not necessarily reflect the views of the NOAA or the US Department of Commerce.

Author contributions

H.M. designed the study, carried out the experiments and analysed the results. G.A.V. and S.W. carried out the experiments and made comments on the manuscript.

Competing interests

The authors declare no competing financial interests.

Additional information

Supplementary information is available for this paper at https://doi.org/10.1038/s41558-017-0008-6.

Reprints and permissions information is available at www.nature.com/reprints.

Correspondence and requests for materials should be addressed to H.M.

Publisher's note: Springer Nature remains neutral with regard to jurisdictional claims in published maps and institutional affiliations.

Methods

Observed data. We used the US Department of Defense Joint Typhoon Warning Center Best Track Database[25], as archived in the International Best Track Archive for Climate Stewardship[26], for the period 1998–2015. The 2016 TC data were complemented in this study by the best track data openly available on the Unisys Corporation website[27]. We also used the UK Met Office Hadley Centre SST product (HadISST1.1) (ref. [28]) as the observed SST. For the atmospheric data, the Japanese 55-year Reanalysis (JRA-55) (ref. [29]) was utilized.

Control experiments. We generated a 600-year control climate simulation using HiFLOR by prescribing the radiative forcing and land-use conditions representative of the year 1860 (1860Cntl). The fixed forcing agents for the control simulations were atmospheric CO_2, CH_4, N_2O, halons, tropospheric and stratospheric O_3, anthropogenic tropospheric sulfates, black and organic carbon, and solar irradiance. We also conducted 1940, 1990 and 2015 control simulations by prescribing the anthropogenic forcing fixed at the levels in those years. Owing to limited computational resources, we ran 1940Cntl, 1990Cntl and 2015Cntl for 200, 300 and 200 years, respectively. However, the basic conclusions were retained even when we used 200 years for all the control simulations.

Empirical probability of exceedance and FAR. To estimate the potential probability of occurrence for the extreme ESCS-incidence years, such as 2015, we examined the empirical probability of exceedance for the frequency:

$$P(x) = \frac{number\ of\ years\ with\ ESCS\ number \geq x}{total\ number\ of\ years} \quad (1)$$

where x is the seasonal mean number of ESCSs in a year. For the control experiments, we compute $P(x)$ using all 600, 200, 300 and 200 simulated years for 1860Cntl, 1940Cntl, 1990Cntl and 2015Cntl, respectively. To elucidate the intercentennial (interdecadal) variability, we computed $P(x)$ for each 50-year (19-year) period.

The FAR[30] was computed for the estimation of the impact of anthropogenic forcing. FAR is defined as follows:

$$FAR(x) = \frac{P(x|E_1) - P(x|E_0)}{P(x|E_1)} \quad (2)$$

where E_1 is the anthropogenic warming condition (for the 1940Cntl, 1990Cntl or 2015Cntl), and E_0 is the natural forcing alone (1860Cntl). FAR ranges from $-\infty$ (not attributable) to 100% (attributable).

To address the impact of any phase of natural variability, we can also estimate the conditional probability of exceedance $P(x|Y_\pm)$ under any phase of a natural mode of variability (that is, Y_+ or Y_-). Here, we investigated the difference in $P(1)$ between positive and negative phases of the El Niño–Southern Oscillation (ENSO), based on the Niño-3.4 index, the Pacific Meridional Mode (PMM)[31], PDO[32] and Indian Ocean Dipole (IOD)[33]. These indices were selected because they may potentially influence the frequency of occurrence of ESCSs based on the SST regression map (Supplementary Fig. 8). The detailed computations for these indices are documented in Murakami et al.[16,17]. In simple terms, ENSO represents the interannual variation of tropical eastern Pacific surface warming concurrent with basin-wide warming in the Indian Ocean, PMM represents the interannual variation of SST warming/cooling over the subtropical eastern Pacific, PDO represents the interannual and decadal variation and IOD represents the interannual variation of the meridional SST contrast in the Indian Ocean. We defined a positive (negative) phase of natural variability when the index was greater than or equal to $+0.75\sigma$ (less than or equal to -0.75σ). The other years were defined as neutral years. $P(x|Y_\pm)$ was computed using the years under each phase.

Projected changes in the Indian monsoon circulation. The projected decrease in V_s may be related to the changes in the strength or the onset of the Indian monsoon. Supplementary Fig. 9 clarifies the changes in the lower/upper tropospheric winds during October–December between the 1860Cntl and 2015Cntl. October–December is the beginning of the South Indian winter monsoon as characterized by northeasterly (southwesterly) winds in the lower (upper) troposphere over the ARB (Supplementary Fig. 1d,e). The projected difference between the 2015Cntl and 1860Cntl indicates a weakening of the winter monsoon circulation: a southwesterly (northeasterly) anomaly in the lower (upper) troposphere over the ARB (Supplementary Fig. 9c–d) leads to a weakening of V_s. However, April–June is the transition season from the winter monsoon to the summer monsoon, as characterized by southwesterly winds in the lower troposphere over the ARB (Supplementary Fig. 1a), which is the opposite to October–December (Supplementary Fig. 1d). The projected difference between the 2015Cntl and 1860Cntl shows a southwesterly flow in the lower troposphere during April–June (Supplementary Fig. 10c). Unlike October–December, the direction of wind change is along the climatological mean wind direction (Supplementary Fig. 10a,c). Moreover, there is less change in the wind in the upper troposphere over the region where ECSCs develop during April–June (Supplementary Fig. 10d), which is one of the major factors for the less-pronounced changes in V_s during April–June relative to October–December (Supplementary Fig. 6c).

Various indices can be used to measure the Indian monsoon. We used the Dynamic Indian Monsoon Index (DIMI) of Wang and Fan[34]. The index is computed by the area mean differences in zonal wind at 850 hPa between regions A (5–15° N, 40–80° E) and B (20–30° N, 70–90° E), denoted in Supplementary Fig. 9a. The index is proportional to the circulation strength, with a positive (negative) value meaning a summer (winter) monsoon phase. We computed the DIMI using the daily data for each 2015Cntl and 1860Cntl run. Also, the DIMI was smoothed with a 15-day running average. Supplementary Fig. 11 shows the smoothed climatological daily DIMI by the 2015Cntl (red) and 1860Cntl (blue), separately. The figure indicates a weakening of both the summer Indian monsoon and winter monsoon from the 1860Cntl to the 2015Cntl. Although the projected DIMI change is significant during the post-monsoon season (October–December), there is no significant difference at a 95% confidence level in the index during the pre-monsoon season (April–June) (Supplementary Table 1). The change of sign occurs almost at the same time between 1860Cntl and 2015Cntl, which indicates the monsoon onset (or withdrawal) occurs almost at the same time in these experiments (Supplementary Fig. 11).

Data availability. The source code of the climate model can be found at https://www.gfdl.noaa.gov/cm2-5-and-flor/; ref. [25]. The data that support the findings of this study are available from the corresponding author on request.

References

25. Chu, J.-H., C. R. Sampson, Levin, A. S. & Fukada, E. *The Joint Typhoon Warning Center Tropical Cyclone Best Tracks 1945–2000* NRL; https://www.gfdl.noaa.gov/cm2-5-and-flor/
26. Knapp, K. R., Kruk, M. C., Levinson, D. H., Diamond, H. J. & Neuman, C. J. The international best track archive for climate stewardship (IBTrACS): unifying tropical cyclone best track data. *Bull. Amer. Meteorol. Soc.* **91**, 363–376 (2010).
27. *Unisys Weather Hurricane/Tropical Data* (UNISYS, 2017); http://weather.unisys.com/hurricane/
28. Rayner, N. A. et al. Global analysis of sea surface temperature, sea ice, and night marine air temperature since the late nineteenth century. *J. Geophys. Res.* **108**, 4407 (2003).
29. Kobayashi, S. et al. The JRA-55 reanalysis: general specifications and basic characteristics. *J. Meteorol. Soc. Jpn* **93**, 5–48 (2015).
30. Jaeger, C. C., Krause, J., Haas, A., Klein, R. & Hasselmann, K. A method for computing the fraction of attributable risk related to climate damages. *Risk Anal.* **28**, 815–823 (2008).
31. Chiang, J. C. H. & Vimont, D. J. Analogous Pacific and Atlantic meridional modes of tropical atmosphere–ocean variability. *J. Clim.* **17**, 4143–4158 (2004).
32. Mantua, N. J., Hare, S. R., Zhang, Y., Wallace, J. M. & Francis, R. C. A Pacific interdecadal climate oscillation with impacts on salmon production. *Bull. Amer. Meteorol. Soc.* **78**, 1069–1079 (1997).
33. Saji, N. H., Goswami, B. N., Vinayachandran, P. N. & Yamagata, T. A dipole mode in the tropical Indian Ocean. *Nature* **401**, 360–363 (1999).
34. Wang, B. & Fan, Z. Choice of south Asian summer monsoon indices. *Bull. Amer. Meteorol. Soc.* **80**, 629–638 (1999).